Hydrogen-Bond Tuning of Macroscopic Transport Properties from the Neutral Molecular Component Site along the Series of Metallic Organic-Inorganic Solvates (BEDT-TTF)4Re6Se5Cl9.[guest]], [guest = DMF, THF, dioxane]

A. Pénicaud, K. Boubekeur, Patrick Batail, Enric Canadell, P. Auban-Senzier, D. Jerome

Hydrogen-Bond Tuning of Macroscopic Transport Properties from the Neutral Molecular Component Site along the Series of Metallic Organic–Inorganic Solvates $(BEDT\text{-}TTF)_4Re_6Se_5Cl_9$·[guest], [guest = DMF, THF, dioxane]

Alain Pénicaud,† Kamal Boubekeur,† Patrick Batail,*,† Enric Canadell,*,‡ Pascale Auban-Senzier,† and Denis Jérome†

Contribution from the Laboratoire de Physique des Solides, CNRS URA 02, and Laboratoire de Chimie Théorique, CNRS URA 506, Université de Paris-Sud, 91405 Orsay, France

Received May 27, 1992

Abstract: A series of single crystals of tetrakis[3,4,3′,4′-bis(ethylenedithio)-2,2′,5,5′-tetrathiafulvalene]$Re_6Se_5Cl_9$·[guest] (**2a–d**) have been prepared where the monoanion is a hexanuclear chalcohalide rhenium cluster and the neutral guest molecules are dimethylformamide (DMF) in **2a** (monoclinic modification) and **2b** (triclinic modification), tetrahydrofuran (THF) in **2c**, and dioxane in **2d**. All four compounds present the same basic structural organization in which conducting organic cation radical slabs are sandwiched by inorganic cluster monoanion layers. The guest molecules are shown to be selectively incorporated into a single site located at the organic–inorganic interface of these layer-like structures. In compounds **2c** and **2d**, a set of C—H···O hydrogen bonds is found to anchor the THF and dioxane molecules to the organic slabs. Although the four compounds are metallic at room temperature, their electrical conductivity at low temperatures and their degrees of structural ordering are shown to strongly depend upon the size, shape, and symmetry of the neutral guest molecule. The latter induces structural changes which are shown to be associated with significant modifications of the band electronic structures, Fermi surfaces, and ultimately the dimensionality of the materials. Altogether, the activated conductivity behavior observed from 90 K down to low temperatures in the case of the disordered DMF solvates **2a** and **2b** appears at only 50 K in the THF-phase **2c**. The inclusion of dioxane successfully orders the structure in **2d**, and the metallic regime is then found to be sustained down to 4.5 K.

Much is lacking in the comprehension of long-range, directional intermolecular electron flow in the solid state. For example, a largely unanswered question is the role of disorder in molecular solid-state assemblies. Of paramount importance are the concepts of defects and impurities which play a pivotal role in the theory of condensed matter physics and which are lacking sound chemical definitions. Little is known about the chemical and crystallographic nature of defects and impurities and their effective concentration in molecular solids. Low-dimensional conductors are very sensitive to disorder and impurities, although it is now recognized that these are less damaging in two-dimensional (2D) systems.[1] Experimental work in this area has been concerned essentially with the deliberate introduction of defects into otherwise highly ordered conducting solids.[2] By contrast, much less attention has been devoted experimentally to the opposite approach, that is, the synthesis and structural analysis of a series of ever increasingly well-ordered conducting molecular solids of high purity. Thus, for that purpose, there is merit in seeking well-defined chemical compositions associated with highly ordered solid-state structures, be they of significant molecular and architectural complexity. Etter et al. recently demonstrated[3] that in those solids in which intermolecular forces such as van der Waals interactions are weak and nondirectional, the occurrence of directional noncovalent intermolecular interactions such as hydrogen bonds effectively determines the configuration of a set of molecules.[3a,b] In particular, cocrystallization studies were shown to be useful for monitoring competitive interactions and selective recognition processes in the solid state.[3c]

The central issue of this paper is the identification of a single source of structural disorder in the homogeneous series of the

† Laboratoire de Physique des Solides.

‡ Laboratoire de Chimie Théorique.

(1) Berezinskii, V. L. *JETP* **1973**, *65*, 1251. See also: Zuppiroli, L. In *Low Dimensional Conductors and Superconductors*; Jérome, D., Caron, L. G., Eds.; NATO ASI B155; Plenum Press: New York, 1987; pp 307–333.

(2) Thus, for example, *compositional and structural disorder* was generally found to prevent the stabilization of long-range charge density wave (CDW) order in charge-transfer salts.[2a] This is basically due to the pinning of the CDW on the impurities, as directly shown by the observation of interference between the CDW modulation and the Laue scattering in the solid solutions $(TTF)_{1-x}(TSeF)_xTCNQ$ and $(HMTTF)_{1-x}(HMTSF)_xTCNQ$.[2d] Likewise, the chemical and structural defects introduced into the one-dimensional stack upon substitution of two of the selenium atoms for sulfur in bis(tetramethyltetraselenafulvane)hexafluorophosphate are found[2b] to induce a localization of the conducting electrons at 100 K, although a unique quantitative analysis of the Laue diffuse scattering confirms[2c] an absence of any correlated structural defaults, i.e., the occurrence of a perfect disorder in the solid. Other defects are those generated by intense X-ray or electron irradiation.[2c] These are poorly characterized chemically[2f] despite their high efficiency at affecting the electron gas flow in the solid state. Numerous studies have been devoted to the effect of those various kinds of disorder on the collective CDW transport properties.[2g] More recently, the threshold field for the onset of nonlinear conduction was found[2h] to increase linearly with the X-ray irradiation dose in $(TMTSF)_2PF_6$. The same effect is observed with a strong dependence on x in $(TMTSF)_2(AsF_6)_{1-x}(SbF_6)_x$.[2i] (a) Pouget, J.-P. In *Semiconductors and Semimetals*; Conwell, E., Ed.; Academic Press: New York, 1988; Vol. 27. (b) Gotschy, B.; Auban-Senzier, P.; Farrall, A.; Bourbonnais, C.; Jérome, D.; Canadell, E.; Henriques, R. T.; Johansen, I.; Bechgaard, K. *J. Phys. I Fr.* **1992**, *2*, 677. (c) Liu, Q.; Ravy, S.; Pouget, J.-P.; Johannsen, I. B.; Bechgaard, K. *J. Phys. I Fr.*, in press. (d) Ravy, S.; Pouget, J.-P.; Comès, R. *J. Phys. I Fr.* **1992**, *2*, 1173. (e) Zuppiroli, L. In *Semiconductors and Semimetals*; Conwell, E., Ed.; Academic Press: New York, 1988; Vol. 27. (f) Mermilliod, N.; Sellier, N. *J. Phys.* **1983**, C3, *44*, 1353. (g) Grüner, G. *Rev. Mod. Phys.* **1988**, *60*, 1129. (h) Kang, W.; Tomic, S.; Jerome, D. *Phys. Rev. B* **1991**, *43*, 1264. (i) Trætteberg, O; Kriza, G.; Lenoir, C.; Huang, Y.-S.; Batail, P.; Jérome, D. *Phys. Rev. Lett.*, submitted for publication.

(3) (a) Etter, M. C. *Acc. Chem. Res.* **1990**, *23*, 120–126. (b) Etter, M. C.; Urbanczyk-Lipkowska, Z.; Zia-Ebrahimi, M.; Panunto, T. W. *J. Am. Chem. Soc.* **1990**, *112*, 8415–8426. (c) Etter, M. C.; Reutzel, S. M. *J. Am. Chem. Soc.* **1991**, *113*, 2586–2598.

0002-7863/93/1515-4101$04.00/0

title lattice solvates subsequently circumvented by a hydrogen-bond-directed, guest-specific pattern of intermolecular association of the host organic constituents with manifestations on the macroscopic electron delocalization. Our results show that the solvate character, a property of the organic–inorganic (OI) nature of those solids, originates from the neutral guest site preference for the OI interface in the layer-like structure. The degree of disorder of the solvate depends upon the symmetry of the molecular guest. The latter is expressed locally through C—H···O hydrogen bonds. Next, the efficient, directional structural functionality of this set of hydrogen bonds is implemented by the long-range translational symmetry to the whole solid due to its solvate character. These observations are supplemented by a theoretical study which demonstrates that the local, cooperative slipping of the donor molecules, associated with seemingly small but significant modifications of the patterns of intermolecular S···S interactions, are reflected in modifications of the band structure and, hence, the electrical conductivity. Of particular note is the clear enhancement of the band structure response in the vicinity of a van Hove singularity[4] responsible for the high susceptibility of the system to a one- to two-dimensional crossover.

One of our recent interests is the exploration of the lattice architectures obtained when organic cation radicals are associated with large, all-inorganic molecular anions with low-lying, essentially delocalized frontier orbitals.[5-8] An important initial step in this research is the synthesis and full structural characterization of the series of tetrabutylammonium salts[6] of the hexanuclear chalcohalide rhenium cluster anions $[^{n}Bu_4N^+]_n[Re_6(Ch_{8-x}Cl_x)Cl_6]^{n-}$ (Ch = chalcogen = S, Se; x = 1,[6a,b] 2,[6b,c] 3;[6b,c] n = 3,[6b,c] 2,[6b,c] 1[6a,b]). These salts are soluble in polar organic solvents, thus providing a unique entry into a versatile solution chemistry.[5a,6] The solid-state associations between the organic electron-donor molecule BEDT-TTF (3,4,3′,4′-bis(ethylenedithio)-2,2′,5,5′-tetrathiafulvalene, or ET) and the monovalent cluster anion $Re_6Se_5Cl_9^-$ were explored using the electrocrystallization technique. In our initial studies we found that single crystals of two distinct phases with different stoichiometries could be grown, depending upon the proportions of CH_2Cl_2 and DMF in the electrochemical cells. Thus, a 4:1 mixture afforded $(ET)^{\bullet+}(Re_6Se_5Cl_9^-)[DMF]_2$[7] (**1**), a 1:1:2 solvate whose crystal structure analysis indicated that stacks of ET cation radicals, developing across side-by-side S···S interactions along the short molecular axis direction, are isolated in the large inorganic cluster anion framework. This fully ionic and insulating salt, with one localized spin $^1/_2$ per $ET^{\bullet+}$ site, was shown to present a magnetic susceptibility characteristic of uniform, noninteracting one-dimensional Heisenberg chains of spins.[7] An additional characteristic feature of this compound is the presence in the crystals of two solvent molecules located between the cluster anions, each of them held tightly in place by a hydrogen bond formed with its oxygen atom and one hydrogen of the ET molecule ethylene side chains. These important latter features and, in particular, the analysis of the relative orientation and interaction of the neutral molecule and the organic cation radical were mostly overlooked in our previous report and are shown now in Figure 1. The

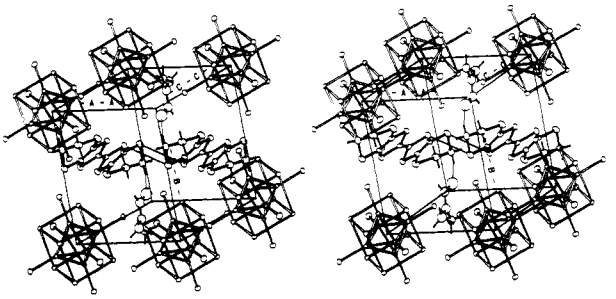

Figure 1. CH···O interaction between $(CH_3)_2NCHO$ and BEDT-TTF in $(ET)^{\bullet+}(Re_6Se_5Cl_9^-)[DMF]_2$ (**1**).

C(H)···O and (C)H···O distances between the carbon atom and the proton nearest the carbonyl group are 3.31 and 2.38 Å, respectively, and the CHO angle is 160.7°.

Electrocrystallization and Chemical Formulation of the 4:1:1 Solvates 2a-d. Increasing the DMF proportion in the solvent mixture yielded platelike twinned crystals. A great many runs were conducted which succeeded at narrowing down the conditions (Table I) for which macroscopic single crystals were found suitable for X-ray data collection and conductivity measurements. Their structure determination in the monoclinic system suggested the presence in the crystal of a solvent molecule so severely disordered that the actual solvent proportion in the formulation could not be determined precisely. In addition, the occurrence of some degree of disorder of one of the six terminal chlorine atoms of the metal cluster resulted in a somewhat poorly resolved structure (R = 0.089) (Table II) as well as numerous unassignable peaks in the residual density map. A comparison by microprobe analysis of the metal/chalcogenide and metal/halide ratios by reference to the 1:1:2 solvate **1** (vide supra) confirmed (Table S1) the formulation of the phase as m-$(ET)_4Re_6Se_5Cl_9$·[DMF] (**2a**, where m refers to monoclinic). The crystals exhibit high room temperature conductivity and metallic behavior (vide infra). The resistivity curve shows a broad minimum around 100 K, typical of a localization of the conducting electrons by some disorder in the material. It was then anticipated that a control of the nature, location, and disorder of the solvent molecule in the structure might result in shifting this resistivity minimum toward lower temperatures or even succeed in sustaining the metallic character down to very low temperatures where the system could eventually enter into a superconducting regime. Additional series of electrocrystallization experiments were then conducted, focusing on the nature and proportions of the mixture of solvents.

When the crystals were grown in the same solvent mixture with additional extreme attention to the purification of DMF, as indicated in Table I, to avoid traces of water and subsequent formation of potentially coordinating dimethylamine, the novel triclinic phase t-$(ET)_4Re_6Se_5Cl_9$·[DMF] (**2b**, where t refers to triclinic) is obtained, and its crystal structure was determined at low temperature. Although the molecule of solvent is still severely disordered in the structure and some additional remaining disorder still affects one of the six terminal chlorine atoms of the cluster anion, the data refinement (R = 0.064 at 140 K) and the significance of the geometry of the ET molecules are considerably improved in this structure when compared to that of **2a**. Microprobe analysis using **1** as a reference (Table S1) revealed that the chemical composition of **2a** and **2b** is identical. We note that the disorder affecting one of the cluster's terminal chlorine atom sites may originate from a loss of a chlorine atom. In fact, analysis of the Fourier map of this site suggested that the terminal chloride may have been displaced by the $(CH_3)_2N$ fragment coming from some decomposition of DMF in the electrochemical cell. No disorder model could be properly refined, however.

In a mixture of THF and CH_3CN, good quality triclinic single crystals are harvested whose density, unit cell volume, and parameters (Table II) are different from, albeit closely related

(4) For an appealing chemist's presentation of the van Hove singularity in the density of states of quasi-two-dimensional systems, see: Wheeler, R. A.; Whangbo, M. H.; Hughbanks, T.; Hoffmann, R.; Burdett, J. K.; Albright, T. A. *J. Am. Chem. Soc.* **1986**, *108*, 2222.

(5) (a) Batail, P.; Boubekeur, K.; Davidson, A.; Fourmigué, M.; Lenoir, C.; Livage, C.; Pénicaud, A. In *The Physics and Chemistry of Organic Superconductors*; Saito, G., Kagoshima, S., Eds.; Springer-Verlag: Berlin, 1990; p 353. (b) Pénicaud, A.; Batail, P.; Coulon, C.; Canadell, E.; Perrin, C. *Chem. Mater.* **1990**, *2*, 123.

(6) (a) Batail, P.; Ouahab, L.; Pénicaud, A.; Lenoir, C.; Perrin, A. *C. R. Hebd. Seances Acad. Sci. Paris* **1987**, *304, Sér II*, 1111–1116. (b) Boubekeur, K. Ph.D. Thesis, University of Rennes, France, 1989. (c) Gabriel, J.-C.; Boubekeur, K.; Batail, P. *Inorg. Chem.*, in press.

(7) Penicaud, A.; Lenoir, C.; Batail, P.; Coulon, C.; Perrin, A. *Synth. Met.* **1989**, *32*, 25–32.

(8) Davidson, A.; Boubekeur, K.; Pénicaud, A.; Auban, P.; Lenoir, C.; Batail, P.; Hervé, G. *J. Chem. Soc., Chem. Commun.* **1989**, 1373.

Table I. Electrocrystallization Conditions

	compd			
	2a	**2b**	**2c**	**2d**
solvent (vol, mL)	DMF (10)/CH_2Cl_2 (15)	DMF (10)/CH_2Cl_2 (15)[a]	THF (25)/CH_3CN (5)	dioxane (10)/CH_3CN (10)
T, °C	21	21	30	30
I, μA	0.7	0.7	1.0	1.0
J, μA cm^{-2}	1.25	1.25	1.80	1.80
ET, mg	25	30	30	17.6
$Et_4NRe_6Se_5Cl_9$, g	0.11	0.16	0.21	
$Bu_4NRe_6Se_5Cl_9$, g				0.15
time, days	12	16	12	10

[a] Dry DMF (SDS, H_2O < 100 ppm) was shaken with alumina (activated at 450 °C for 1 night prior to use) and then distilled under vacuum (t = 32 °C) and passed over activated alumina prior use; dry CH_2Cl_2 (SDS, H_2O < 100 ppm) was passed over activated alumina prior use; both solvents and the electrocrystallization cell were degassed by vacuum–argon cycles on a Schlenk line (see text).

Table II. Crystallographic Data

	compd			
	2a	**2b**	**2c**	**2d**
formula	$Re_6Se_5Cl_9C_{43}S_{32}ONH_{39}$	$Re_6Se_5Cl_9C_{43}S_{32}ONH_{39}$	$Re_6Se_5Cl_9C_{44}S_{32}OH_{40}$	$Re_6Se_5Cl_9C_{43}S_{32}O_2H_{40}$
formula weight	3442.9	3442.9	3441.9	3457.9
crystal dimens, mm	0.33 × 0.15 × 0.02	0.27 × 0.10 × 0.06	0.27 × 0.18 × 0.02	0.24 × 0.18 × 0.03
crystal color	black	black	black	black
T, K	293	140	293	293
crystal system	monoclinic	triclinic	triclinic	triclinic
space group	$P2_1/m$	$P\bar{1}$	$P\bar{1}$	$P\bar{1}$
a, Å	10.409(2)	10.338(1)	9.059(1)	9.050(3)
b, Å	36.542(4)	18.308(3)	20.311(2)	20.254(7)
c, Å	11.572(1)	11.489(1)	11.680(1)	11.766(7)
α, deg	90.0	95.62(2)	84.58(1)	84.63(4)
β, deg	105.44(1)	105.24(2)	102.19(1)	102.63(4)
γ, deg	90.0	82.13(2)	79.32(1)	78.99(3)
V, Å^3	4242(2)	2070(11)	2042(6)	2045(26)
Z	2	1	1	1
d_{calcd}, g cm^{-3}	2.70	2.76	2.74	2.81
d_{measd}	2.70			
$F(000)$	3114	1557	1557	1605
μ, cm^{-1}	124	127	123	123
detector aperture, mm	2.0 + 0.5 tan θ	1.3 + 0.5 tan θ	1.5 + 0.5 tan θ	1.4 + 0.5 tan θ
scan type	ω	ω/θ	$\omega/2\theta$	$\omega/2\theta$
scan width, deg	1.35 + 0.35 tan θ	0.6 + 0.35 tan θ	0.9 + 0.35 tan θ	0.8 + 0.35 tan θ
absorption correction	ψ scans	ψ scans + difabs	ψ scans	ψ scans
$2\theta_{max}$, deg	54	56	52	54
data collected	9920	10297	8416	9356
independent data	9412	9986	8003	8909
observed data ($I_{obs} \geq 3\sigma(I)$)	3315	6123	5259	5684
guest atoms	c	c	isotropic	anisotropic
hydrogen atoms	c	c	riding	riding
parameters refined	193	415	427	442
R^a	0.089	0.064	0.041	0.033
$R_w{}^a$	0.121	0.101	0.056	0.051
goodness of fit[b]	2.27	2.92	1.63	1.08
final shift/error residual	0.00	0.01	0.00	0.00
d, e Å^{-3}	6.27	5.60	2.02	1.77

[a] $R = \||R_o| - |F_c|\|/|F_o|$. $R_w = [w(|F_o| - |F_c|)^2/w|F_o|^2]^{1/2}$. [b] GOF = $[w(|F_o| - |F_c|)^2/(N_{observations} - N_{variables})]^{1/2}$. [c] Not included. See Experimental Section.

Table III. Cluster Inner-Ligand Multiplicity in **2b**, **2c**, and **2d**

	compd		
	2b[a]	**2c**	**2d**
μ_{Se1}	0.88	0.86	0.82
μ_{Se2}	0.84	0.70	0.70
μ_{Se3}	0.67	0.92	0.91
μ_{Se4}	0.62	0.94	0.91
B_{iso}	2.36	2.47	2.28

[a] Note that the numbering scheme for the cluster anion is different in **2b** than in the other two structures.

Table IV. Cluster Inner-Ligand Multiplicity in **2a** and Subsequent Site Assignment

site labeling	local symmetry	μ_{theor} (pure Se)	μ_{obs}	B_{iso}	L_i atom assignment
1	m	0.5	0.47	3.41	Se1
2	1	1	0.88	3.41	Se2
3	1	1	0.57	3.41	Cl5
4	m	0.5	0.43	3.41	Se4
5	m	0.5	0.21	3.41	Cl6
6	m	0.5	0.39	3.41	Se3

to, those of **2a,b**. The resolution and analysis of the crystal structure, which includes the location of one THF molecule per formula unit, and the good quality of the data refinement (R = 0.041) lead to the chemical formulation $(ET)_4Re_6Se_5Cl_9$·[THF] (**2c** or **2**·[THF]) and demonstrate that the structural ordering has been significantly improved in the material. In particular, each terminal chlorine atom of the cluster anion was found to be well-behaved in the refinement, leaving no ambiguity about the actual cluster composition in the material. In fact, the only remaining disorder originates from the molecule of THF, selectively incorporated from the solvent mixture, the intrinsic disorder affecting the inner chalcogen/halogen cluster anion sites not withstanding. Indeed, the solvate molecule is constrained to sit on the centrosymmetrical guest site in the solvate and therefore exhibits inversion disorder.

Table V. BEDT-TTF···Guest C—H···O Interactions[a] in **2c** and **2d**

	2c			2d		
(C)H···O (Å)	2.55 (2.46)	2.58 (2.49)	2.84 (2.78)	2.71 (2.62)	2.67 (2.56)	3.05 (2.98)
C(H)···O (Å)	3.29	3.36	3.43	3.45	3.46	3.65
∠CHO (deg)	134.6 (132.6)	139.2 (137.2)	120.7 (118.3)	134.9 (132.8)	141.0 (140.1)	123.0 (121.0)

[a] The contact distances and angles are calculated with C–H distances of 0.95 Å and (1.08 Å),[34] respectively.

Table VI. Relevant Interatomic Distances (Å), Averaged in O_h Symmetry, within the Cluster Anion in **1**, $^nBu_4NRe_6Se_5Cl_9$ (**1'**), and **2a–d**

	compd					
	1	**1'**	**2a**	**2b**	**2c**	**2d**
Re–Re (Å)	2.610(3)	2.607(1)	2.574(16)	2.580(5)	2.613(4)	2.608(4)
Re–L_i (Å)	2.500(6)	2.498(2)	2.48(4)	2.50(3)	2.51(1)	2.502(9)
Re–Cl_i (Å)	2.360(8)	2.353(3)	2.415(6)	2.404(7)	2.372(8)	2.365(6)

The electrocrystallization experiments were then conducted, substituting dioxane for THF in the solvent mixture assuming that their similar size, shape, and oxygen functionalities will favor the selective accommodation and achieve the structural ordering of the former centrosymmetrical molecule in the host lattice. Large, well-shaped platelike single crystals were obtained. They were the best quality crystals grown in the series, and the determination of their structure ($R = 0.033$) indeed verified that the material is perfectly ordered with the expected formulation $(ET)_4Re_6Se_5Cl_9$·[dioxane] (**2d** or **2**·[dioxane]).

A Common Structural Principle for 2a–d. Stereoscopic views of the unit cell contents of **2a–d** are shown in Figures 2a–d, respectively. A distinctive feature of their structural chemistry is readily apparent when these structures are compared with that of the 1:1:2 salt **1**, illustrated in Figure 1. All four salts adopt the same type of structure in which layers of donor molecules and inorganic cluster anions alternate along the *b* axis direction, normal to the larger, well-developed face of the platelike crystals. Note that the layer character of these structures is actually found in most salts of this particular organic donor. In that respect, the structure of **1** is a notable exception.

The π-framework of the donors is typically more inclined with respect to the inorganic layer in the DMF solvates **2a** and **2b** than in **2**·[THF] and **2**·[dioxane], suggesting that the C–H bonds at both ends of the donor molecules are different in the two sets of salts. Also, not only is the *b* axis significantly longer in **2c** and **2d** (Table II), as expected, but, in addition, in the latter no contraction occurs along *b* upon cooling (Table VII). Therefore, this evidence of a quite remarkably stiffer stacking of the layers in the dioxane phase **2d** is a clear indication that the solvate structure has been properly locked in upon incorporation of dioxane in the guest cavity.

Another important feature exemplified by these structures is the stability of such $(ET)_n$ layers against significant increases of the size of the inorganic counteranions, regardless of their charge. This supplements our recent observation of a similar sandwich structure for $(ET)_8SiW_{12}O_{40}$, a remarkable two-dimensional salt[8] of the tetravalent and considerably larger Keggin anion. Actually, in most instances such ET layers tend to be associated[9a] with the magic 2:1 stoichiometry adopted by the metallic salts of considerably smaller, either discrete or polymeric monovalent anions, whose prominent examples are β-$(ET)_2I_3$[9a,10a,b] or κ-$(ET)_2Cu(NCS)_2$[10c,d] and κ-$(ET)_2[Cu(NCN)_2Br]$.[10e] The stoichiometries determined for these novel families of hybrid organic–inorganic salts strikingly demonstrate that the 2:1 ratio can simply be increased to adjust to the size of the inorganic molecule. Clearly, the unique structural stability of this two-dimensional π-network is associated with the size and shape of its molecular constituent. As emphasized previously,[11] the latter are best expressed by two structural functionalities of the donor molecule, namely, the number of sulfur atoms in the π-framework and the conformational flexibility of the ethylene end groups which enhance the possibilities of C—H···anions as well as C—H···S contacts in a variety of directions at the outskirts of the molecule. Perhaps the most important structural consequence of the latter property is that it makes the molecule nonplanar, thereby favoring intermolecular patterns of interactions of higher, essentially two-dimensional character.

It is of interest to observe that the strong tendency of the tetrathiafulvalenium cation radicals to form stacks along the normal to their molecular plane cannot be satisfied when the cation radical is associated with $Re_6Ch_5Cl_9^-$. Rather, in $(TTF)_2^{\bullet+}Re_6Ch_5Cl_9^-$ [6b,12] the stack breaks down into a pattern of discrete mixed-valence dimers or even, as in $(TTF^{+\bullet})_3Re_6S_6Cl_8^{2-}(Cl^-)$, into a three-dimensional dispersion of discrete cation radicals, embedded in a unique perovskite structure.[13] By contrast, the nature of the single-chain arrangement of $Et^{\bullet+}$s observed in **1**, where orbital interaction occurs preferentially across intermolecular S···S contacts in the transverse direction, testifies for the stability of these in-plane contacts which are still effective even when direct overlap of the π-system normal to the molecular plane cannot be sustained. As can be clearly seen in Figure 1, the availability of twice as many sulfur atoms in the ET molecule as in TTF has favored this extra, strong capability of the ET cation radicals to couple along the transverse direction. Therefore, what drives the two-dimensional arrangement in **2a–d**? We suggest that the major, significant difference between the two types of structures is to be found in the differences in the patterns of C—H···O(guest) and C—H···anions interactions between **1** and **2**, just as the reason for the remarkable two-dimensional sandwich structure of $(ET)_8SiW_{12}O_{40}$ has been attributed to a set of C—H···O(anions) contacts probing the oxygen sites at the interface of the Keggin anion arrays.[8] As a result, the π-systems of the ET molecules have been forced back in **2a–d** into relative positions where they can interact directly, hence the two-dimensional character of the structure in contrast to **1**. These novel observations in comparatively very different situations support the recent rationalization by Whangbo et al.[11] of the key

(9) (a) Williams, J. M.; Wang, H. H.; Emge, T. J.; Geiser, U.; Beno, M. A.; Leung, P. C. W.; Carlson, K. D.; Thorn, R. J.; Schultz, A. J.; Whangbo, M.-H. In *Progress in Inorganic Chemistry*; Lippard, S. J., Ed., Interscience: New York, 1987; Vol. 35, pp 51–218. (b) Williams, J. M.; Wang, H. H.; Emge, T. J.; Geiser, U.; Beno, M. A.; Leung, P. C. W.; Carlson, K. D.; Thorn, R. J.; Schultz, A. J.; Whangbo, M.-H. In *Progress in Inorganic Chemistry*; Lippard, S. J., Ed., Interscience: New York, 1987; Vol. 35, p 91.

(10) (a) Yagubskii, E. B.; Schegolev, I. F.; Laukhin, V. N.; Komonovich, P. A.; Kartsovnik, A. V.; Zvarykina, A. V.; Buravov, L. I. *Pis'ma Zh. Eksp. Teor. Fiz.* **1984**, *39*, 12; *JETP Lett. (Engl. Transl.)* **1984**, *39*, 12. (b) Shibaeva, R. P.; Kaminskii, V. F.; Yagubskii, E. B. *Mol. Cryst. Liq. Cryst.* **1985**, *119*, 361. (c) Urayama, H.; Yamochi, H.; Saito, G.; Nozawa, K.; Sugano, T.; Kinoshita, M.; Sato, S.; Oshim, K.; Kawamoto, A.; Tanaka, J. *Chem. Lett.* **1988**, 55. (d) Urayama, H.; Yamochi, H.; Saito, G.; Sato, S.; Kawamoto, A.; Tanaka, A.; Mori, T.; Maruyama, Y.; Inokuchi, H. *Chem. Lett.* **1988**, 463. (e) Kini, A. M.; Geiser, U.; Wang, H. H.; Carlson, K. D.; Williams, J. M.; Kwok, W. K.; Vandervoort, K. G.; Thomson, J. E.; Stupka, D. L.; Jung, D.; Whangbo, M.-H. *Inorg. Chem.* **1990**, *29*, 2555.

(11) (a) Whangbo, M.-H.; Jung, D.; Ren, J.; Evain, M.; Novoa, J. J.; Mota, F.; Alvarez, S.; Williams, J. M.; Beno, M. A.; Kini, A. M.; Wang, H. H.; Ferraro, J. R. In *The Physics and Chemistry of Organic Superconductors*; Saito, G., Kagoshima, S., Eds.; Springer-Verlag: Berlin, Heidelberg, 1990; pp 262–266. (b) Novoa, J. J.; Mota, F.; Whangbo, M.-H.; Williams, J. M. *Inorg. Chem.* **1991**, *30*, 54–58. (c) Novoa, J. J.; Whangbo, M.-H.; Williams, J. M. *Chem. Phys. Lett.* **1991**, *180*, 241.

(12) Boubekeur, K.; Livage, C.; Batail, P., to be published.

(13) Batail, P.; Livage, C.; Parkin, S. S. P.; Coulon, C.; Martin, J. D.; Canadell, E. *Angew. Chem., Int. Ed. Engl.* **1991**, *30*, 1498.

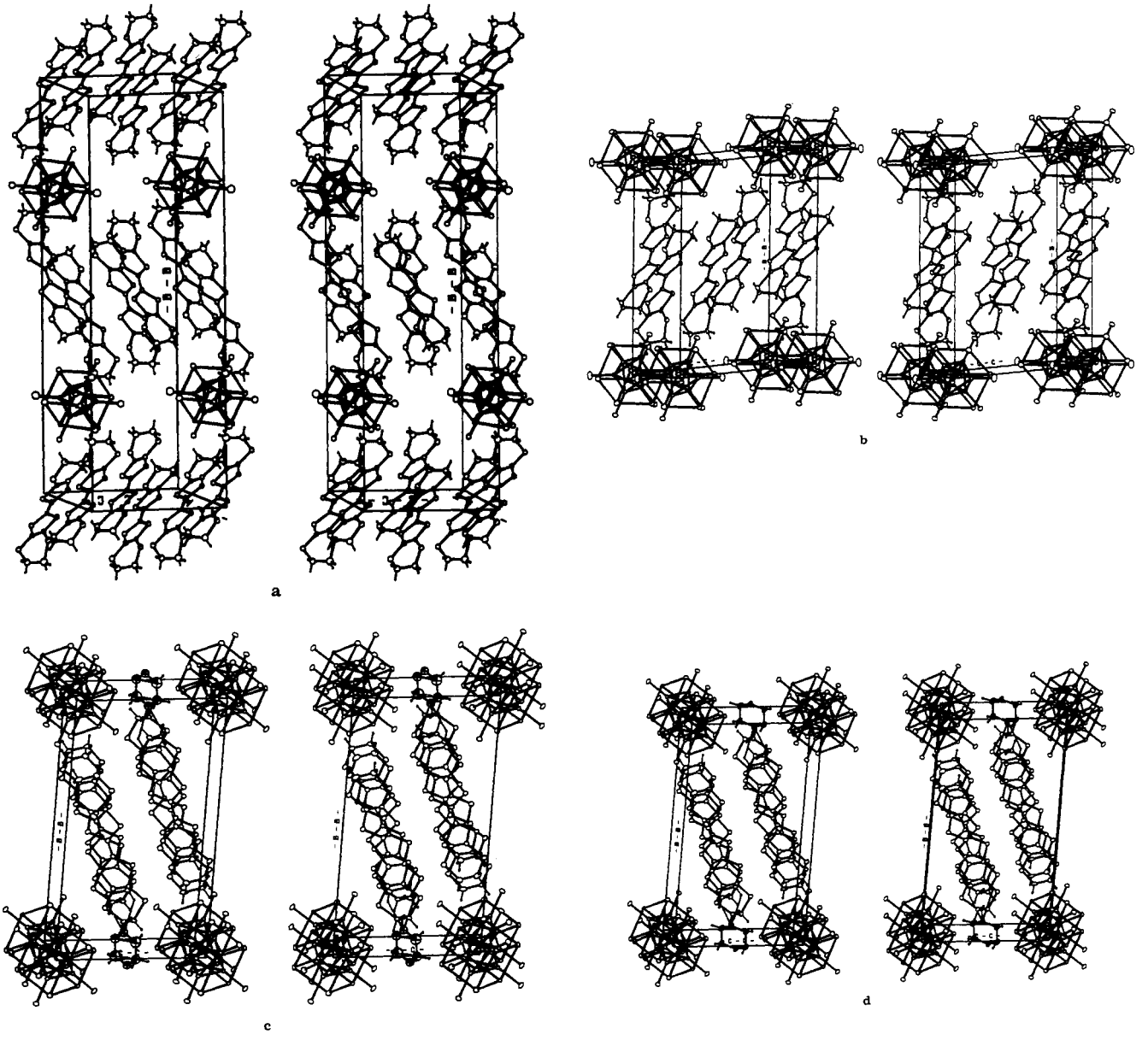

Figure 2. Stereoscopic view of the structures of (a) m-$(ET)_4Re_6Se_5Cl_9$·[DMF] (**2a**); (b) t-$(ET)_4Re_6Se_5Cl_9$·[DMF] (**2b**); (c) $(ET)_4Re_6Se_5Cl_9$·[THF] (**2c**); and (d) $(ET)_4Re_6Se_5Cl_9$·[dioxane] (**2d**).

Table VII. Comparison of the Unit Cells of **2a–d** at Different Temperatures

	compd						
	2a	**2a** one-half[a]	**2b**	**2b**	**2c**	**2d**	**2d**
t (K)	293	293	293	140	293	293	140
space group	$P2_1/m$	$P\bar{1}$	$P\bar{1}$	$P\bar{1}$	$P\bar{1}$	$P\bar{1}$	$P\bar{1}$
a (Å)	10.409(2)	10.409	10.446(1)	10.338(2)	9.059(1)	9.050(3)	8.928(3)
b (Å)	36.542(4)	18.427	18.373(3)	18.308(3)	20.311(2)	20.254(7)	20.256(6)
c (Å)	11.572(1)	11.572	11.598(1)	11.489(3)	11.680(1)	11.766(7)	11.655(2)
α (deg)	90.0	95.01	94.95(1)	95.62(2)	84.58(1)	84.63(4)	85.00(2)
β (deg)	105.44(1)	105.44	105.56(1)	105.24(2)	102.19(1)	102.63(4)	102.32(2)
γ (deg)	90.0	83.34	82.80(1)	82.13(2)	79.32(1)	78.99(3)	78.54(3)
V (Å^3)	4242(2)	2121	2124(5)	2070(11)	2042(6)	2045(26)	2000(17)

[a] Cell calculated by linking the clusters centers by the three shorter non-colinear vectors.

role of C—H···anion interactions in determining the structure of ET cation radical salts. We conclude, then, that in the present and related organic–inorganic hybrid salts, those interactions are responsible for the observed two-dimensional character, and we suggest that their efficiency is particularly enhanced by the nonplanarity of the molecule, which softens its otherwise strong tendency to overlap preferentially along the direction normal to the molecular plane.

It is also of interest to comment upon the unique charge balance achieved in **2a–d**, a consequence of the monovalent character of the inorganic molecular cluster. Note that the high donor:anion ratios achieved with di- and tetraanions in $(ET)_4Mo_6Cl_{14}[THF]_2$[14]

(14) (a) Fuchs, H. Ph.D. Thesis, University of Münich, Germany, 1988. (b) Amberger, E.; Fuchs, H.; Polborn, K. *Synth. Met.* **1987**, *19*, 605. (c) Fuchs, H.; Fuchs, S.; Polborn, K.; Lehnert, Th.; Heidmann, C.-P.; Müller, H. *Synth. Met.* **1988**, *27*, A271.

and $(ET)_8SiW_{12}O_{40}$, respectively, still satisfy the usual $^1/_2$ average charge per ET molecule. In **2a–d**, the highest charge dilution yet stabilized in single ET layers is obtained, which makes them particularly low Madelung energy salts. Quite interestingly, however, this low charge concentration in the layer is associated with an electron count leaving a half-filled band structure (vide infra) especially favorable to metallic conductivity, while, for the same reason, $(ET)_4Mo_6Cl_{14}[THF]_2$ is insulating with a gap at the Fermi level.

The Chalcohalide Cluster Anion $Re_6(Se_{i5}Cl_{i3})(Cl_t)_6^-$. Formulation and Charge. The molecular cluster anions adopt in all four structures the expected geometry,[6b,7,15] that is, an Re_6 octahedron surrounded by a distribution of five selenium and three chlorine atoms on its eight face-capping sites (Figures 2 and S1). The latter, labeled as inner ligands[16] L_i (Table VI), can be viewed as located at the vertices of the cubic motif enclosing the octahedron (Figure 2). Note that this is merely a convenient pictorial representation of the cluster motif with no indication of any chemical bonding across the vertices of the cube connecting discrete ligand sites. Six rhenium-bonded terminal chlorides (Cl_t) complete the 14-ligand set of the Re_6 unit as in the classical isostructural and isoelectronic, albeit divalent, molybdenum halide clusters $Mo_6X_{14}^{2-}$ (X = Cl, Br, I).

Extensive structural correlations in the series $Re_6(Ch_{8-x}Cl_x)Cl_6^{n-}$ (x = 3, 2, 1; n = 1, 2, 3) have demonstrated[6] that the rhenium-to-ligand bond lengths, and most notably the Re–Cl_t distances, are indicative of the actual charge of the anion. The relevant interatomic distances within the cluster anions in **2a–d** as well as the corresponding distances in **1** and $^nBu_4NRe_6Se_5Cl_9$ (**1'**) are given in Table VI. The agreement is satisfactory for the ordered structure of **2d** only, while the lack of accuracy precludes any meaningful correlation between selected bond lengths and the actual charge of the cluster anion in **2a,b**. Note, however, that the chemical formulation $Re_6(Se_{i5}Cl_{i3})(Cl_t)_6$ is independently verified by the successful refinements for all four structures of composite, diffusion-factor-weighted inner ligands, as discussed in the Experimental Section.

Conformational Isomers, Accidental Centrosymmetry, and Dipolar Character. Of particular note is the intrinsic disorder of these inorganic molecular ions associated with the presence, both in solution and in the solid state, of all of the possible noncentrosymmetrical conformational isomers resulting from the distribution of five chalcogen and three chlorine atoms onto the eight face-capping positions coordinating the Re_6 octahedron. Therefore, a dissymmetrical charge distribution surrounds the metal cluster, which then presents an intrinsic dipole moment. In the solid state, the cluster anions in **2b–d** are located on centers of symmetry and are therefore locally disordered (Table III). The site symmetry for the cluster anion in **2a** is m, and some degree of ordering of the cluster anion was observed in the structure refinement (Table IV and Figure S2).

The Guest Cavity. The pseudo-close-packed arrangement of the chalcohalide cluster anion layers creates holes of significant volume, i.e., translational symmetry-related cavities are interspersed into the lattice (Figure 2). Each cavity is delineated on both sides along the transverse direction by ethylene end groups of ET molecules and is found to host a single neutral guest molecule, selectively incorporated from the solvent mixture during the electrocrystallization. This is illustrated for **2**·[dioxane] in Figure 3.

Size–Shape Selectivity. The actual cross sections of cavities are 29.4, 30.0, 16.7, and 17.2 Å^2 for **2a–d**, respectively. These are defined as the surfaces of the a,c faces of their unit cells less the surface of the a,b face (86.7 Å^2) in **1**,[7b] taken as a reference for the closest packing of such anions in the absence of a neutral guest (Figure 1). Note that DMF (Figure 1) and dioxane (Figure 2d) or the inversion-disordered pseudo-THF (Figure 2c), while of different shapes, are comparable in size (Chart I). For the present purpose, we will simply observe that their long and short molecular axes are equivalent to linear sequences of four and three sp^3 atoms, respectively. Also, they are very similar in volume since they possess essentially the same number of atoms. Therefore, the actual cross section difference observed between the cavities in **2a,b** and **2c,d** is a manifestation of the differences in the orientation of the neutral guests only. Clearly, THF and dioxane are standing their long molecular axes up in the cavities in **2c** (Figure 2c) and **2d** (Figures 2d and 3), where their molecular planes are essentially normal to the layers. Thus, the diameter of the cavities, 4.6 Å, may be taken as that of the neutral molecules across their shorter molecular axis and may be thought of as the equivalent of a sequence of three sp^3 atoms. The actual cross section for the cavities in **2a** and **2b** is ca. 30 Å^2, that is, nearly twice that of the cavities in **2c** and **2d** (17 Å^2). Likewise, this yields a cavity diameter of 6.2 Å for **2a,b** which is then expected to fit a molecular length equivalent to a sequence of four sp^3 atoms. These results imply that DMF is able to lie with its long molecular axis in the equatorial plane of the cavities in **2a** and **2b**.

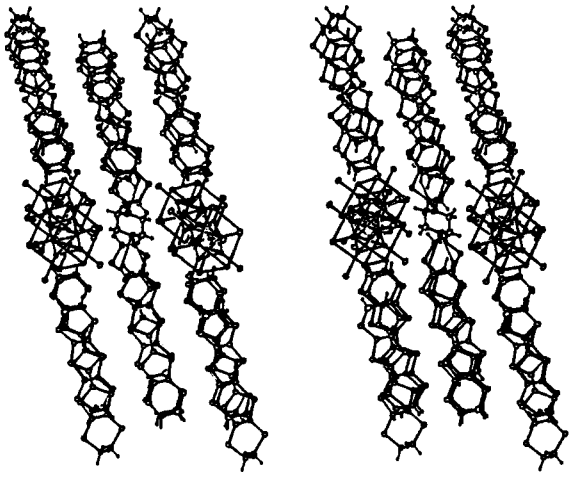

Figure 3. Binding of dioxane in **2d**.

Chart I

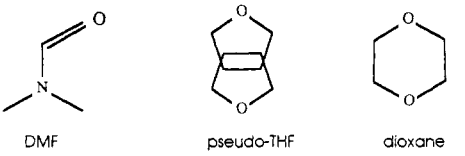

Hydrogen-Bond Pattern Analysis. There is no proton available to properly lock the amide carbonyl oxygen when DMF is lying in the equatorial (cluster) plane of the cavities. We suggest that the latter is in fact large enough to accommodate the guest in many different orientations, hence the observed severe disorder reminiscent of recent examples by Cram and co-workers[17] demonstrating that incarcerated DMF rotates rapidly around all three axes on the ^{1}H NMR time scale, even at some low temperature.

On the contrary, the ethereal oxygen atoms of dioxane in **2d** as well as those of the inversion-disordered THF in **2c** protude out from the inorganic layer toward ethylene groups of ET molecules (Figure 3). The interactions associated with the dioxane or THF oxygens are not only characteristic of this set of structures but are also the key to understanding the exquisite structural specificity in the construction of **2c** and **2d**. Three C—H···O contacts are identified (Table V, Figures 2 and 3). The orientation

(15) Leduc, L.; Perrin, A.; Sergent, M. *C. R. Hebd. Seances Acad. Sci. Paris* **1983**, *296, Sér. II*, 961.
(16) Schäfer, H.; Schnering, H. G. *Angew. Chem.* **1964**, *76*, 833.
(17) Sherman, J. C.; Knobler, C. B.; Cram, D. J. *J. Am. Chem. Soc.* **1991**, *113*, 2194–2204.

and geometry of these two sets of contacts are very similar between the two compounds. Note that the lengths of the contacts in **2c** are shorter than the lengths of the corresponding contacts in **2d**. We believe that this difference is merely a consequence of the somewhat unrealistically larger size of the disordered pseudo-THF molecule imposed to fit on this site in **2c**. Although two of the C···O lengths are shorter (Table V), all three distances fall in the expected range[18a,b] for such weak interactions. The two shorter H···O separations observed compare very satisfactorily with the recently calculated value of 2.58 Å.[18c] In fact, for those primarily electrostatic C—H···O interactions, which fall off very slowly with distance,[11,18a] very small energy differences are associated with comparatively large variations of the bond distances. Thus, conformational adaptations occur readily to maximize the *number* of interactions, even at the expense of an increase of the interaction distances. Therefore, we conclude, in agreement with a recent survey by Desiraju,[18a] that the C—H···O hydrogen-bonding interactions listed in Table V should be considered significant.

Centrosymmetrical Oxygen Bifunctionality Required. It was indeed the recognition that inversion disorder of the solvent molecule enabled a proper hydrogen-bond coupling of the ET molecules across the inorganic layer along the transverse *b* axis direction in **2c** (Figure 2c) that prompted the choice of dioxane as electrocrystallization cosolvent and the subsequent synthesis of **2d** with a highly ordered structure (Figures 2d and 3). This indicates that the degree of ordering of solvates depends upon the symmetry of the guest molecule. While inversion disorder appears to be a feature common to many solvates and lattice clathrates,[19] it is shown here that local as well as long-range ordering of the structures in the present series is achieved by using a guest molecule with two inversion-related ethereal oxygen atoms.

Guest-Specific Pattern of Association within the Organic Layer. There are two crystallographically unique BEDT-TTF molecules (A and B) per asymmetric unit in all four materials. The projections down the long axis of the molecules of single organic layers of t-$(ET)_4Re_6Se_5Cl_9$·[DMF] (**2b**) and $(ET)_4Re_6Se_5Cl_9$·[dioxane] (**2d**), shown in Figures 4 and 5, respectively, appear very similar and of the *Z*-mode type.[9b] Nevertheless, this similarity is only apparent and specific for this particular projection of the layers.[20] In fact, the centroids of BEDT-TTF molecules in one slab are not coplanar but rather are displaced off the projection plane in such a way that the patterns of association of the molecules in the transverse direction, i.e., looking normal to the BEDT-TTF molecular planes at 90° angles to the present projections, are different and specific to the nature of the guest. In order to analyze these features further, it is important to recognize first that any slab is assembled by side-by-side interactions of collinear stacks of ET molecules overlapping along the *a* direction with an offset of one-half of the short in-plane molecular axis. Note that the latter is a common feature of the stacks in all four structures. Of particular note also is the observation that segregated stacks of molecules A and B are found in **2a** and **2b** (Figure 4) and mixed stacks of A and B are observed in **2c** and **2d** (Figure 5). Then it appears, again for all four compounds, that the stacks consist of the repetition of dimers, as exemplified in Figures 6 and 7. The single and highly significant difference between the slab organization in the DMF solvates **2a** and **2b** and that of the THF and dioxane solvates **2c** and **2d** is to be found in the difference in the amount of interdimer slipping

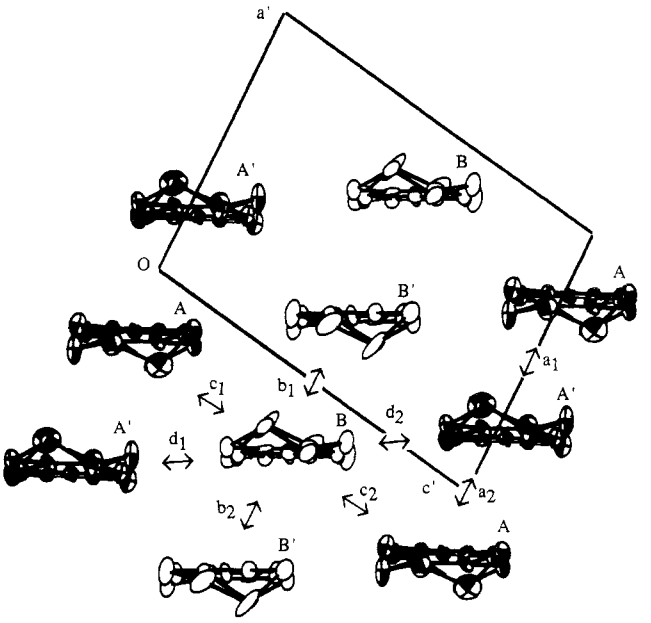

Figure 4. Pattern of association within the organic slab as viewed down the BEDT-TTF long molecular axis in **2b**. a_1–d_2 denote the interaction types between pairs of BEDT-TTF, as defined in Table VIII. (Oa'c') is the projection of (Oac).

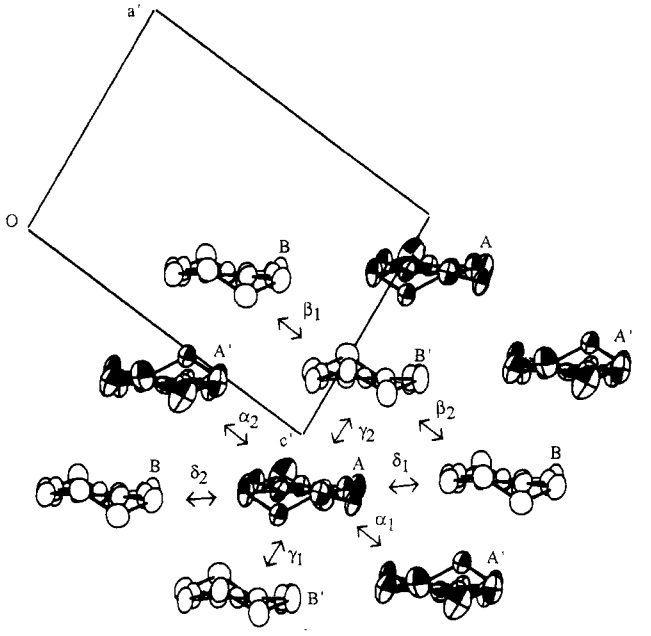

Figure 5. Pattern of association within the organic slab as viewed down the BEDT-TTF long molecular axis in **2d**. α_1–δ_2 denote the interaction types between pairs of BEDT-TTF, as defined in Table IX. (Oa'c') is the projection of (Oac).

along the long molecular axis, as demonstrated in Figures 8. Indeed, the interdimer slipping in **2b** is as large as one-half the long molecular axis length (Figure 8a), that is, essentially twice that observed in **2d** (Figure 8b).

This remarkable, guest-specific difference in the interdimer slipping and slab organization has some striking consequences (Figure 6 and 7) on the interslab mode of association, namely, the size of the solvate cavities, the inclination of the organic cation radical planes to the inorganic layers, and the three-dimensional distribution of the cluster anion sites.

The Guest Oxygen Bifunctionality Pulls the Slabs Closer. Indeed, the dioxane molecule happens to be exquisitely fitted in its cavity (Figure 7), where the donor molecule CH groups reach out toward the oxygen atoms of dioxane, as exemplified by the

(18) (a) Desiraju, G. R. *Acc. Chem. Res.* **1991**, *24*, 290–296. (b) Note that the C···O lengths of the two donor–acceptor C—H···O interactions which have been shown to drive the structural phase transition accompanying the electronic neutral-to-ionic transition in tetrathiafulvalene–chloranil are 3.37 and 3.45 Å: Batail, P.; La Placa, S. J.; Mayerle, J. J.; Torrance, J. B. *J. Am. Chem. Soc.* **1981**, *103*, 951. (c) Wiberg, K. B.; Waldron, R. F.; Schulte, G.; Saunders, M. *J. Am. Chem. Soc.* **1991**, *113*, 971–977.

(19) Byrn, M. P.; Curtis, C. J.; Goldberg, I.; Hsiou, Y.; Kahn, S. I.; Sawin, P. A.; Tendick, S. K.; Strouse, C. E. *J. Am. Chem. Soc.* **1991**, *113*, 6549–6557.

(20) The layer organizations for **2a** and **2c** are identical to those of **2b** and **2d**, respectively, and are not represented.

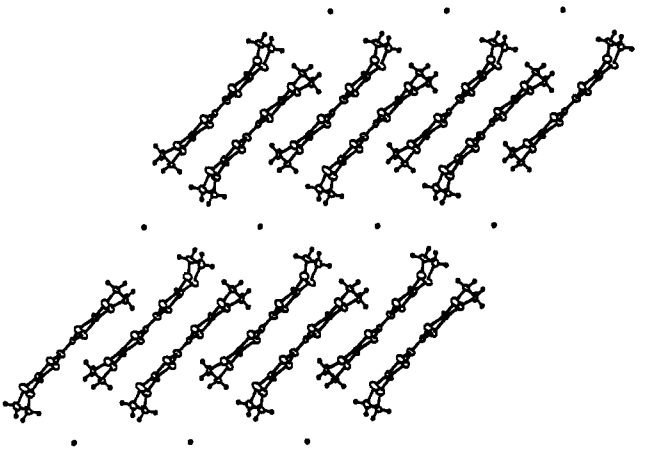

Figure 6. Interslab mode of association as viewed essentially down the short in-plane BEDT-TTF molecular axis in **2b**.

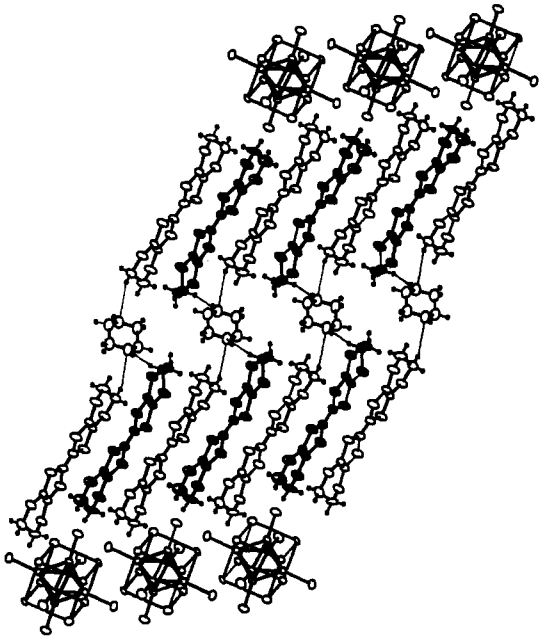

Figure 7. Interslab mode of association as viewed essentially down the short in-plane BEDT-TTF molecular axis in **2d**.

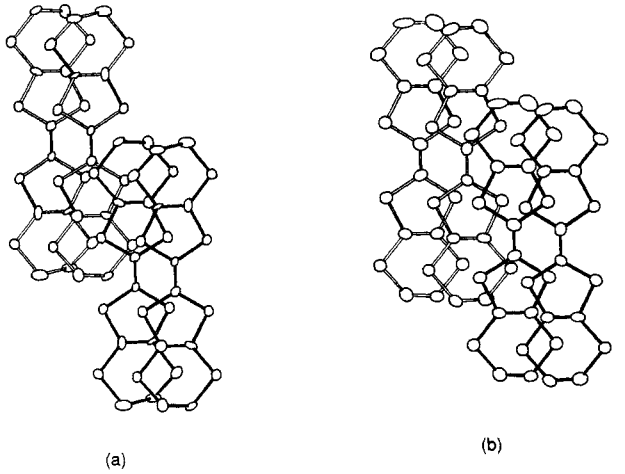

Figure 8. Intra- and interdimers overlap along the stack in one slab in (a) **2b** and (b) **2d**.

adoption of *different* and, in that respect, very appropriate configurations of the ethylene ends of the two closer donor molecules belonging to successive dimers in a given slab. By

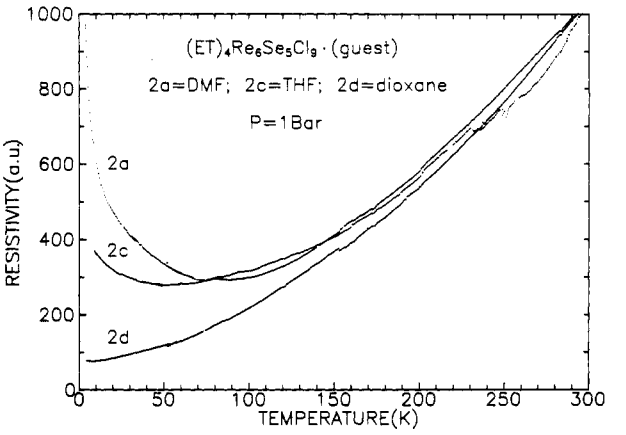

Figure 9. Temperature dependence of the single crystal resistivities of **2a**, **2c**, and **2d** at ambient pressure.

contrast, there is no need for the dimers to slip along in **2b** since no oxygen atom is available for bonding there (Figure 6), hence a larger cavity. In addition, it is worth pointing out not only that the conformation of the opposite ethylene end groups, that is, those facing the cluster anion sites in **2d** (Figure 7), differs from the conformation of those engaged in CH···O hydrogen bonding, but also that this conformation is uniform in agreement with the occurrence of a somewhat equally uniform distribution of CH···Cl donor anion interactions.

Guest-Specific Inclination of the Organic Cation Radical Slabs. The neutral guest molecules and cluster anion centroids belong to the *a,c* plane in all four structures. The angles between the ET molecular planes and the latter are, on the average, 56° in **2a** and **2b** and 64° in **2c** and **2d**. As can be clearly seen by comparing Figures 6 and 7, when centrosymmetrical oxygen atoms are absent in the solvate cavity a collective inclination of the organic cation radical slab occurs.

Guest-Specific Distribution of the Cluster Anion Sites. A final and striking difference between the two sets of compounds is found in the mode of distribution of the guest molecule and cluster anion sites along the ET long molecular axis direction. In **2c** and **2d**, a single sequence takes place in which a guest site and a cluster anion site alternate (Figure 7). In **2a** and **2b**, however, the ethylene end groups of the ET molecules only face either a guest molecule or a cluster anion (Figures 2a,b and 6). Thus, the crystal structures could be described by considering either the stacking, along the short BEDT-TTF in-plane axis, of ET slabs mixed with guest molecules and cluster anions as in **2c** and **2d** or that of successive segregated guest molecule- or cluster anion/ET slabs as in **2a** and **2b**.

Transport Properties. All four compounds exhibit high room temperature conductivities and metallic behavior. Their single crystal electrical conductivities at ambient pressure and room temperature are similar, typically 20–60 S cm^{-1}. When the temperature is decreased, an activated behavior appears in a temperature range which is decreasing with the amount of disorder in the structures. Specifically, a broad minimum in the resistivity curve is observed at ca. 90 K for **2a**, the most severely disordered material. It is shifted down to 50 K for **2c** and has essentially vanished in **2d** (Figure 9). Of particular note is the observation that the leveling off of the resistivity curve remains small and is increasingly weaker when the temperature of the resistivity minimum decreases. All these features are strong indications of an electron localization as a consequence of disorder effects rather than the occurrence of a phase transition driven by a charge density wave (CDW) or a spin density wave (SDW) commonly observed[2a,g] in low-dimensional conductors.

Additional transport measurements conducted on single crystals of **2a** under an applied pressure of 16 kbar demonstrated that the

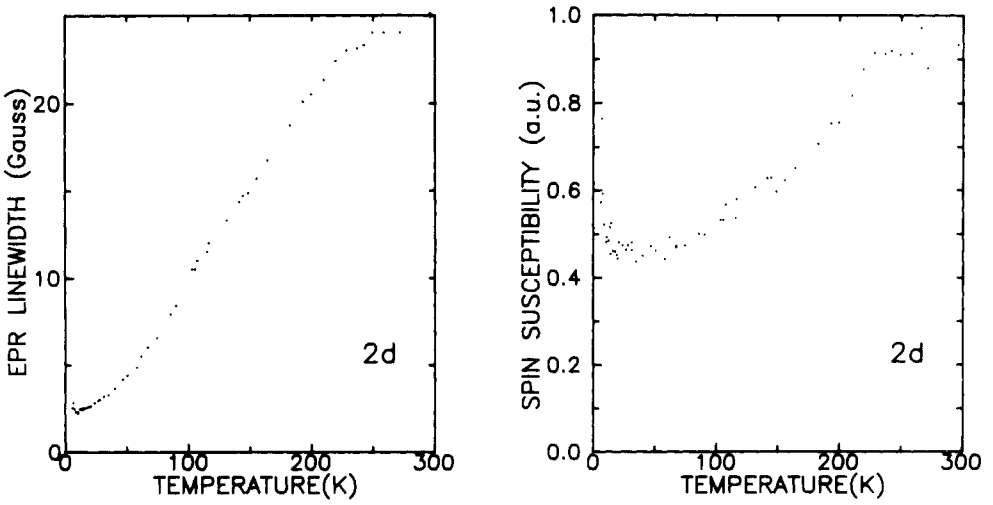

Figure 10. Temperature dependences of ESR line width and spin susceptibility measured on a single crystal of **2d**.

localization minimum was considerably flattened and shifted down to 30 K. Also, we found that no superconductivity regime was observed upon the application of a pressure of 10 kbar in **2d**.

ESR Measurements. A single crystal ESR line width of 25 G is found at room temperature for **2d**. It decreases down to 2.5 G at 8 K (Figure 10a). The spin susceptibility (Figure 10b) follows the resistivity down to ca. 40 K, where a saturation occurs followed by a slight upturn below 10 K. While for a purely 2D metal the spin susceptibility remains essentially independent of the temperature, as has been verified in the case of β-(BEDT-TTF)$_2$I$_3$,[21] the observation of a continuous decrease in the spin susceptibility with temperature in **2d** (Figure 10b) suggests that the electron gas flow is essentially one-dimensional (1D) in nature in this material and hence particularly sensitive to disorder and impurities. Indeed, the data in Figure 10b are very reminiscent of the temperature dependence of the susceptibility in 1D conductors such as those belonging to the (TMTSF)$_2$X series. The temperature dependence of the spin susceptibility of conducting and superconducting members of the (TMTSF)$_2$X series is very close indeed to the behavior observed[22] for the (TMTTF)$_2$X series, which undergoes a Mott–Hubbard localization at low temperatures. The similarity between temperature dependences of χ_s in 1D conductors and 1D quantum antiferromagnets is a clear manifestation of the spin–charge separation of the one-dimensional interacting electron gas.

The absence of any long-range order at low temperature due to the onset of an SDW state suggests that **2d** is potentially a good candidate for a superconducting ground state, i.e., the transverse coupling $t_\perp$ is large enough to prevent the establishment of the competing instability, namely the SDW ground state. However, since the present ESR study as well as the analysis of the band structure calculations reported below emphasizes the quasi-1D nature of **2d**, superconductivity, if it exists at all, would be expected at a rather low temperature, typically 2 K at the most, as for the superconducting Bechgaard salts.[23]

Band Electronic Structures. Since the 2D *structural* character of the materials is clearly identified in the analysis of their crystal structures, it is of interest to analyze their electronic structures to appreciate the origin of the likely 1D character of **2d**. The energies of the highest occupied molecular orbitals (HOMOs) of the two different BEDT-TTF molecules of the four slabs (i.e., the orbitals leading to the partially filled bands) are quite similar and all lie in a narrow energy range of 0.2 eV. As a consequence, the HOMO bands of the four slabs will result from a strong mixing of the HOMOs of both molecules A and B. The calculated band structures for the BEDT-TTF slabs of **2a**, **2b**, and **2d** are shown in Figure 11a, b, and c, respectively. The band structure for the BEDT-TTF slab of **2c** is practically identical to that shown in Figure 11c.

Since the unit cells of all slabs contain four BEDT-TTF molecules (two of type A and two of type B), there are four HOMO bands. With the formal oxidation required by the stoichiometric formula, i.e., (BEDT-TTF)$_4^+$, there are seven electrons per unit cell to fill the bands of Figure 11. As shown there, the Fermi level associated with this filling cuts only the highest-lying band, which, consequently, is half-filled. In all cases, this band has a sizable dispersion (0.3–0.4 eV), so the four materials are expected to be metallic, in agreement with our conductivity measurements.

As shown in Figure 11, the partially filled band of all slabs is dispersive along both the a^* (i.e., along $\Gamma \rightarrow$ X) and c^* (i.e., along $\Gamma \rightarrow$ Z) directions. However the dispersion along a^* is smaller. As a consequence, the Fermi level of the BEDT-TTF slabs of **2a** (Figure 11a) and **2d** (Figure 11c) does not cut the upper band along the a^* direction, leading to the open Fermi surfaces of Figures 12a and c, respectively. Interestingly, the Fermi level for the BEDT-TTF slab of **2b** (Figure 11b) cuts the upper band in all directions, leading to the closed Fermi surface of Figure 12b. Note that the monoclinic $P2_1/m$ unit cell of **2a** contains *two* BEDT-TTF slabs. As a consequence, assuming that the tunneling interaction between the slabs is negligible, the true Fermi surface of the system should be the superposition of *two* Fermi surfaces like that of Figure 12a. Since the two BEDT-TTF slabs are related by a 2_1 screw axis along b, the two separate pieces coincide and the Fermi surface of Figure 12a can be considered the real Fermi surface of the system.

According to the results of Figures 11 and 12, although the electronic interactions along the different directions of the a,c plane are quite sizable, the phases **2a**, **2c**, and **2d** should be pseudo-1D materials with better conductivity along the c direction, whereas **2b** should be a 2D metal. Pseudo-1D materials often present metal–insulator transitions associated with either CDW or SDW formation.[24] When one piece of the Fermi surface can be translated by a vector **q** and superposed onto another piece of the Fermi surface, the two pieces are said to be nested by **q**. The CDW or SDW instabilities typically occur when the Fermi surface of the material is nested. Except for the regions near the X point, the Fermi surfaces of Figures 12a and c have a pseudoellipsoid shape and are not well nested. Therefore, our calculations suggest

(21) Rothaemel, B.; Forro, L.; Cooper, J. R.; Schilling, J. S.; Weger, M.; Bele, P.; Brunner, H.; Schweitzer, D.; Keller, H. J. *Phys. Rev. B.* **1986**, *34*, 704.

(22) Coulon, C. In *Organic and Inorganic Low Dimensional Crystalline Materials*; Delahes, P., Drillon, M., Eds.; NATO ASI Series; Plenum Press: New York, 1987; pp 201.

(23) Jérome, D.; Creuzet, F.; Bourbonnais, C. *Phys. Scr.* **1989**, *127*, 130.

(24) Jérome, D.; Schulz, H. J. *Adv. Phys.* **1982**, *31*, 299.

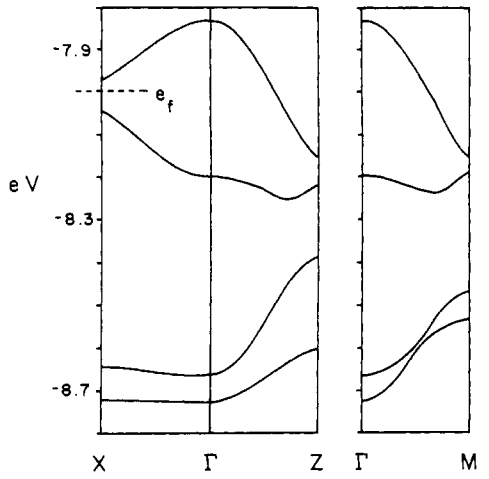

(a)

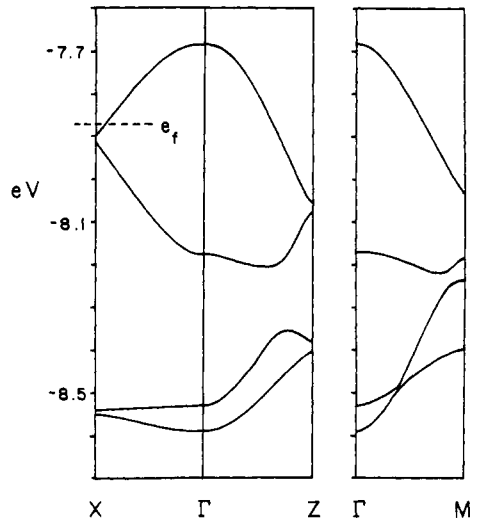

(b)

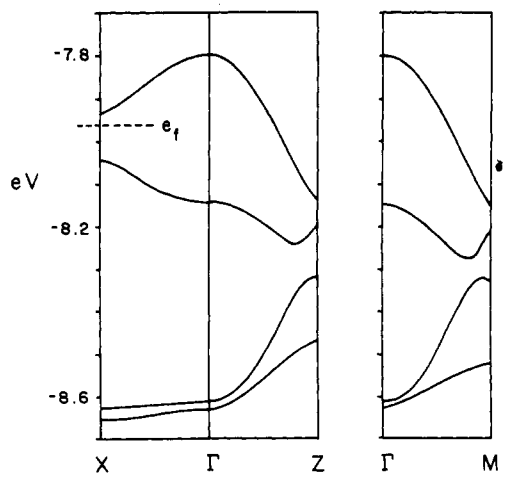

(c)

Figure 11. Band structure calculated for the BEDT-TTF slabs of (a) m-(BEDT-TTF)$_4$Re$_6$Se$_5$Cl$_9$·[DMF] (**2a**); (b) t-(BEDT-TTF)$_4$Re$_6$Se$_5$Cl$_9$·[DMF] (**2b**); and (c) (BEDT-TTF)$_4$Re$_6$Se$_5$Cl$_9$·[dioxane] (**2d**). Γ, X, Z, and M refer to the wave vectors (0, 0), ($a^*/2$, 0), (0, $c^*/2$), and ($-a^*/2$, $c^*/2$), respectively. The dashed line refers to the Fermi level.

that the low-temperature upturn shown in the resistivity curves is not due to CDW or SDW but to disorder-induced localization. This is consistent with the transport and ESR measurements as well as the fact that the resistivity upturn occurs at lower temperatures for **2c** and **2d** where solvent disorder has been suppressed and only the intrinsic cluster disorder remains.

It is interesting to inquire about the origin of the different Fermi surface calculated for the BEDT-TTF slab of **2b** (Figure 12b). In order to approach this problem, we calculated the different interaction energies β[25] associated with the BEDT-TTF HOMO. The interaction energy between orbitals i and j (β_{ij}) is written as (1), where $c_{\mu i}$ is the coefficient of atomic orbital χ_μ in

$$\beta_{ij} = \sum_{\mu}\sum_{\nu} c_{\mu i} c_{\nu j} \langle \chi_\mu | H^{\text{eff}} | \chi_\nu \rangle \quad (1)$$

$$\psi_i = \sum_{\mu} c_{\mu i} \chi_\mu \quad (2)$$

the molecular orbital ψ_i (2). These interaction energies have been widely used by Whangbo et al.[25] to discuss the electronic structure of BEDT-TTF-based molecular conductors. As shown in Figure 4 for the BEDT-TTF slabs of **2a,b** and in Figure 5 for those of **2c,d**, there are eight different types of interactions between the BEDT-TTF molecules. The corresponding $\beta_{\text{HOMO-HOMO}}$ interaction energies are reported in Tables VIII and IX.

The BEDT-TTF slabs of m- and t-(ET)$_4$Re$_6$Se$_5$Cl$_9$·[DMF] both have chains of the same type of BEDT-TTF molecules (i.e., A or B) parallel to the a direction (see Figure 4). Comparison of the β values for the m and t salts **2a** and **2b**, respectively, (Table VIII) shows that the main difference between the two slabs lies in the intrachain interactions and, more specifically, those of molecules B. In that case, one of the two interactions (b_2) is extremely weak in the m salt. The interchain interactions (A–B) are very similar in the two slabs. As noted above, the HOMO bands result from a very strong mixing of the HOMOs of molecules A and B. In fact, a detailed analysis of the crystal orbitals of the partially filled band for different points of the Brillouin zone shows that there is an almost equivalent participation of the HOMOs of molecules A and B. It is then quite easy to understand that if one of the transfer integrals along the chain is very weak, the dispersion along this direction will be smaller than those associated with interchain directions, leading to an anisotropic behavior. The main reason why interaction b_2 is weaker in the m salt **2a** seems to be associated with the S1B–S3B contacts, which are 0.13 Å longer (3.83 vs 3.70 Å, see supplementary material) in this salt. Although the distance criteria can be misleading when trying to understand the strength of different interactions, here we are comparing two situations in which the relative orientation between the two partners is practically the same so that the comparison is meaningful. Since the S1 and S3 sites are associated with strong orbital coefficients

(25) (a) Whangbo, M.-H.; Williams, J. M.; Leung, P. C. W.; Beno, M. A.; Emge, T. J.; Wang, H. H. *Inorg. Chem.* **1985**, *24*, 3500. (b) Since overlap is explicitly included in extended Hückel calculations, these interaction energies β should not be confused with the conventional transfer integrals t. Although the two quantities are obviously related and have the same physical meaning, the absolute values of β are somewhat greater than those of t.

(26) Larsen, J.; Lenoir, C. *Synthesis* **1989**, *2*, 134. Larsen, J.; Lenoir, C. *Org. Synth.* **1993**, in press.

(27) Atomic scattering factors were obtained from the following: *International Tables for X-ray Crystallography*; Kynoch Press: Birmingham, England, 1974; Vol. IV.

(28) Frenz, B. A. *Computing in Crystallography*; Delft University Press: Delft, The Netherlands, 1978.

(29) Whangbo, M.-H.; Hoffmann, R. *J. Am. Chem. Soc.* **1978**, *100*, 6093.

(30) Hoffmann, R. *J. Chem. Phys.* **1963**, *39*, 1397.

(31) Ammeter, J. H.; Bürgi, H.-B.; Thibeault, J.; Hoffmann, R. *J. Am. Chem. Soc.* **1978**, *100*, 3686.

(32) (a) Whangbo, M.-H.; Williams, J. M.; Leung, P. C. W.; Beno, M. A.; Emge, T. J.; Wang, H. H.; Carlson, K. D.; Crabtree, G. W. *J. Am. Chem. Soc.* **1985**, *107*, 5815. (b) Clementi, E.; Roetti, C. *At. Nucl. Data Tables* **1974**, *14*, 177.

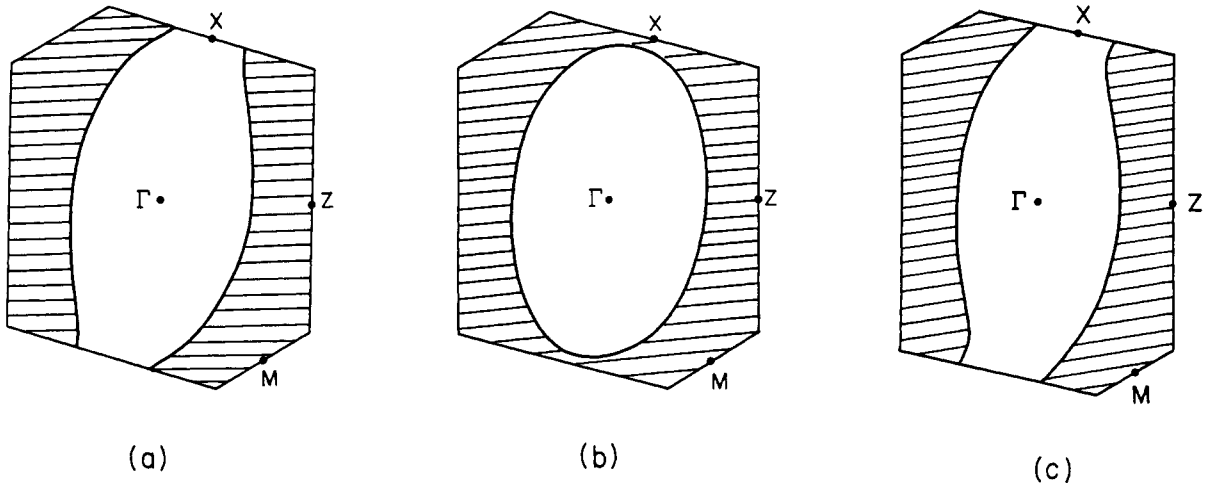

Figure 12. Fermi surfaces associated with the half-filled band of (a) m-(BEDT-TTF)$_4$Re$_6$Se$_5$Cl$_9$·[DMF] (**2a**); (b) t-(BEDT-TTF)$_4$Re$_6$Se$_5$Cl$_9$·[DMF] (**2b**); and (c) (BEDT-TTF)$_4$Re$_6$Se$_5$Cl$_9$·[dioxane] (**2d**). The wave vectors of the shaded and unshaded regions refer to filled and unfilled band levels, respectively.

Table VIII. Absolute Values of the $\beta_{HOMO-HOMO}$ Interaction Energies (eV) for the BEDT-TTF Slabs of **2a** and **2b**

interaction type[a]	2a	2b
a_1	0.0841	0.0880
a_2	0.1319	0.0925
b_1	0.0569	0.1083
b_2	0.0013	0.1268
c_1	0.1762	0.1685
c_2	0.2990	0.2943
d_1	0.1291	0.1425
d_2	0.1260	0.1416

[a] For labeling see Figure 4.

Table IX. Absolute Values of the $\beta_{HOMO-HOMO}$ Interaction Energies (eV) for the BEDT-TTF Slabs of **2c** and **2d**

interaction type[a]	2c	2d
α_1	0.1507	0.1335
α_2	0.3045	0.2988
β_1	0.2641	0.2514
β_2	0.2720	0.2689
γ_1	0.0785	0.0832
γ_2	0.0591	0.0445
δ_1	0.1198	0.1159
δ_2	0.1154	0.1148

[a] For labeling see Figure 5.

in the HOMO of BEDT-TTF,[25a] as schematically shown in **3**, differences in the S1B–S3B distances will have a noticeable effect in the interaction energies.

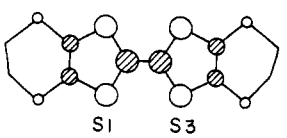

3

Comparison of the interactions in the BEDT-TTF slabs of **2b** and those of **2c** or **2d** seem less obvious because in the latter there are chains of A–B–A–B type parallel to the *a* direction (see Figure 5) instead of chains A–A–A–A and B–B–B–B in the former (see Figure 4). However, comparison of the β values of Tables VIII and IX shows that the interaction energies are quite similar except for the pairs β_1 vs c_1 and γ_2 vs a_2 or b_2. According to these values, the interactions along *c* should be stronger in **2c** or **2d**, whereas those along *a* should be weaker. Thus the BEDT-TTF slabs in **2c** or **2d** should be more anisotropic than those in **2b** and have a stronger dispersion along the *c* direction. This ultimately leads to the open Fermi surface of Figure 12c and accounts for the similarity in electronic structure between the donor slabs of **2a**, **2c**, and **2d** in spite of the structural differences.

The three Fermi surfaces of Figure 12 are very similar except for the region around the X point. It is worth mentioning that the X point lies in a minimum of the dispersion along this line and very near to the Fermi level (~0.03 eV). Thus a slight perturbation of the calculated dispersion relations could result in a change from closed to open Fermi surface or vice versa. Under such conditions it is obvious that the calculated Fermi surfaces depend very sensitively on the structural and computational details. Although, as shown in Figure 12, large portions of the Fermi surface would not be affected by such a change, it would be of great interest to have an experimental proof of the open or closed nature of the Fermi surface. Unfortunately, magnetoresistance measurements for **2b** can be not quite appropriate because of the existence of some disorder. Our ESR measurements suggest that these phases are indeed pseudo-1D. However, what is quite clear is that slight structural changes in these phases can change the Fermi surface from open to closed or vice versa. Since in this process the X point becomes the locus of a van Hove singularity in the density of states, the physical properties of these and related materials are very exciting to study.

Concluding Remarks. After a period of intense debate, the weak, essentially electrostatic C—H···O interactions have been recognized only very recently as common and perhaps very effective at governing the orientation of molecules in the solid state.[18a] Examples of their role in electroactive molecular solids are scarce. They have been shown to be the dominating intermolecular interaction in the construction of the structure of the salts derived from bis(ethylenedioxy)tetrathiafulvalene,[11a,33] to impose the unique acentric structure of (BEDT-TTF)$_8$-SiW$_{12}$O$_{40}$,[8] and to be associated with a structural phase transition going along the neutral-to-ionic transition in tetrathiafulvalene–chloranil.[18b] Thus, by imposing the architecture of the solid, they may be considered to play a significant, albeit indirect, role on the electronic properties of those compounds although their actual implication or coupling with the latter remains to be examined in depth. Here, C—H···O hydrogen bonding has been

(33) Suzuki, T.; Yamochi, H.; Srdanov, G.; Hinkelmann, K.; Wudl, F. *J. Am. Chem. Soc.* **1989**, *111*, 3108. See also: Wudl, F.; Yamochi, H.; Suzuki, T.; Isotalo, H.; Fite, C.; Liou, K.; Kasmai, H.; Srdanov, G. In *The Physics and Chemistry of Organic Superconductors*; Saito, G., Kagoshima, S., Eds.; Springer-Verlag: Berlin, Heidelberg, 1990; pp 358–363.

(34) As pointed out by Churchill, the use of a C–H distance of 0.95 Å in crystal structure refinements tends to produce a better fit of the X-ray data, although calculations using a distance of 1.08 Å should give more realistic contact separations: Churchill, M. R. *Inorg. Chem.* **1973**, *12*, 1213. We thank one referee for suggesting that we calculate those separations using the latter C–H distance also.

shown to be central to the interplay of structural ordering, electron delocalization, and band structure singularity in a unique series of metallic solvates of organic–inorganic character.

Experimental Section

Synthesis of $(C_2H_5)_4N(Re_6Se_5Cl_9)$ and $(C_4H_9)_4N(Re_6Se_5Cl_9)$. The following detailed procedure involves first the synthesis of $KRe_6Se_5Cl_9$,[15] which is then dissolved in alcohol where metathesis with the corresponding alkylammonium chloride is achieved.[6a] This synthetic sequence, only briefly described previously, is reported here in appropriate detail. Re (0.918 g, 4.93 mmol), Se (0.389 g, 4.93 mmol), KCl (0.134 g, 1.80 mmol), and $ReCl_5$ (0.892 g, 2.45 mmol) were ground together and pressed into a pellet inside a drybox. The pellet was introduced into a quartz tube which was then sealed under vacuum after three argon–vacuum cycles. The pellet was heated to 800 °C over 14 h and kept at that temperature for 10 h. The resulting powder was a mixture of $KRe_6Se_5Cl_9$, Re, and K_2ReCl_6. The latter is water soluble and was eliminated by stirring the mixture in acidified water at 20 °C for 3 h and filtering. The solid residue was dried overnight and then stirred in ethanol for several days at room temperature to give an orange solution. The undissolved powder (Re) was filtered off. Upon addition of an ethanolic solution containing an excess of Et_4NCl (or Bu_4NCl), $Et_4NRe_6Se_5Cl_9$ ($Bu_4NRe_6Se_5Cl_9$) was precipitated, filtered, and washed with EtOH. Starting with a total of 1.374 g of Re (Re + $ReCl_5$), the procedure yielded 0.77 g of $Et_4NRe_6Se_5Cl_9$ (57%).

Crystallization of m-$(ET)_4Re_6Se_5Cl_9$·[DMF], t-$(ET)_4Re_6Se_5Cl_9$·[DMF], $(ET)_4Re_6Se_5Cl_9$·[THF], and $(ET)_4Re_6Se_5Cl_9$·[dioxane]. BEDT-TTF was prepared following the Larsen–Lenoir synthesis[26] and recrystallized three times in toluene. Black shiny platelets of each cation radical salt were grown at platinum wire anodes under constant-current electrolysis of solutions of BEDT-TTF and the corresponding tetraethyl- or tetrabutylammonium salt, as detailed in Table I. All solvents were dried over activated alumina before use. Semiquantitative elemental analyses of **1**, **2a**, and **2b** were carried out by energy-dispersive X-ray microanalysis with a scanning electron microscope (Table S1).

X-ray Diffraction Study. X-ray Weissenberg and Precession photographs indicate that the single crystals of **2a** have a monoclinic symmetry and that many are twinned with a pseudotriclinic unit cell. Precise unit cell dimensions and intensity data were collected on a CAD4-F diffractometer, equipped with a nitrogen stream for **2b**, using graphite monochromated Mo Kα radiation (λ = 0.710 73 Å). The structures were solved by Patterson and Fourier techniques.[27] The weighting scheme used was $1/w = [\sigma^2(I) + (0.07F_o^2)^2]/4F_o^2$ with $\sigma(I)$ from counting statistics. All computer programs are from the Enraf–Nonius structure determination package.[28] Crystal data, details of the data collection, and structure solving for single crystals of **2a–d** are listed in Table II. As discussed in the text, DMF is highly disordered and could not be located in **2a** and **2b**. Therefore, the structure refinements were conducted in both cases without solvent or hydrogen atoms. In **2c** and **2d**, the hydrogen atoms were included as riding atoms with a fixed C–H distance of 0.95 Å. In **2c**, a model of two centrosymmetrically related THF molecules, centered at ($^1/_2$, 0, $^1/_2$), was refined isotropically and proved satisfactory. Finally, dioxane is properly located in **2d** and refined anisotropically (Figure S1).

The eight inner-ligand cluster anion sites are occupied by a distribution of five selenium and three chlorine atoms, and the subsequent disorder was treated as follows. After isotropic refinement of the whole structure using selenium scattering factors for all eight inner ligands, the multiplicities of these ligands were refined (still using the selenium scattering factors) together with the isotropic thermal factor of one of them, the thermal factors of the other seven ligands being reset to the refined value after each cycle. This is based on the assumption that such inner ligands, being in the same intramolecular arrangement, have approximately the same isotropic thermal factors. Thus, if one of the inner-ligand sites is occupied by a higher proportion of chlorine than selenium, it should be reflected in its multiplicity. In fact, chlorine having 17 electrons against 34 for selenium, a chlorine atom should appear as a selenium atom with 0.50 multiplicity in the refinements. The results are presented in Table III for **2b–d**. In these triclinic phases where the cluster anion is located on an inversion center, no site discrimination is recognized and the final refinements are performed using uniform inner ligand L_i equivalent to $^5/_8$ selenium atom and $^3/_8$ chlorine atom with a scattering factor scaled accordingly. In the monoclinic salt **2a** the cluster anion is located on a mirror plane and two inner ligands reach a multiplicity close to half of the expected value for a pure selenium site, the other ones having their multiplicity close to the pure selenium value (Table IV). According to the local symmetry of the ligands, this leads to the expected formulation Se_5Cl_3. The final refinement was then performed with the subsequent ordered model of selenium and chlorine atoms, as indicated in Figure S2. The somewhat high (low) value of the isotropic thermal factor of Se3 (Cl5) reflects only the deviation of the reality from the proposed model.

Conductivity Measurements. The temperature dependence of the conductivity of all the materials was measured on single crystals at ambient pressure using a four-probe dc technique with gold evaporated contacts from 295 to 4.2 K and up to 16 kbar for **2a** and 10 kbar for **2d**. The isostatic pressure-transmitting liquid was isopentane.

ESR Measurements. Single crystal temperature-dependent ESR measurements were performed on a Varian X-band spectrometer (9.3 GHz) from 295 to 4.2 K.

Band Structure Calculations. The tight-binding band structure calculations[29] were of the extended Hückel type.[30] A modified Wolfsberg–Helmholz formula was used to calculate the nondiagonal $H_{\mu\nu}$ values.[31] Double-ζ orbitals[32] for C and S were used. The exponents (ζ_μ and ζ_μ') and weighting coefficients (c_μ and c_μ') of the double-ζ orbitals and $H_{\mu\mu}$ (eV) values used were 1.831, 1.153, 0.7616, 0.2630, and −21.4 for C 2s; 2.730, 1.257, 0.2595, 0.8025, and −11.4 for C 2p; 2.662, 1.688, 0.5564, 0.4874, and −20.0 for S 3s; and 2.328, 1.333, 0.5208, 0.5439, and −13.3 for S 3p.

Acknowledgment. We warmly thank the European Community (DGXIII) Basic Research Action for Grant MOLCOM 3121, which supported this work.

Supplementary Material Available: Numbering scheme for the four structures; data for m-$(ET)_4Re_6Se_5Cl_9$·[DMF] (tables of atomic coordinates (including calculated hydrogen atoms (C–H distance = 0.95 Å)) and isotropic thermal factors, interatomic bond lengths and angles, and H···L (L = Se, Cl) intermolecular contacts less than 3.5 Å), t-$(ET)_4Re_6Se_5Cl_9$·[DMF] (tables of atomic coordinates (including calculated hydrogen atoms (C–H distance = 0.95 Å)), anisotropic thermal parameters, interatomic bond lengths and angles, and H···L (L = Se, Cl) intermolecular contacts less than 3.5 Å), $(ET)_4Re_6Se_5Cl_9$·[THF], and $(ET)_4$-$Re_6Se_5Cl_9$·[dioxane]; numbering scheme for the cluster anion in m-$(ET)_4Re_6Se_5Cl_9$·[DMF] (Figure S1); interatomic distances and angles in the dioxane molecule (Figures S2); observed and calculated atomic percentages in S, Cl, Re, and Se (Table S1) (50 pages); listing of observed and calculated structure factors for the four compounds (197 pages). Ordering information is given on any current masthead page.